EFDA–JET–PR(09)03

YQ Liu, I.T. Chapman, S. Saarelma, M.P. Gryaznevich, T.C. Hender,
D.F. Howell and JET EFDA contributors

An Improved Method to Evaluate the Ideal No-Wall Beta Limit from Resonant Field Amplification Measurements in JET

An Improved Method to Evaluate the Ideal No-Wall Beta Limit from Resonant Field Amplification Measurements in JET

JET-EFDA, Culham Science Centre, OX14 3DB, Abingdon, UK

[1]EURATOM-UKAEA Fusion Association, Culham Science Centre, OX14 3DB, Abingdon, OXON, UK
** See annex of F. Romanelli et al, "Overview of JET Results",*
(Proc. 22 [nd] IAEA Fusion Energy Conference, Geneva, Switzerland (2008)).

Preprint of Paper to be submitted for publication in
Plasma Physics and Controlled Fusion

ABSTRACT.
Modelling the low-n, low frequency Resonant Field Amplification (RFA) effects for JET plasmas, using the MHD code MARS-F, offers explanations to one of the recent observations made in experiments, namely a mismatch between the measured RFA threshold and the predicted no-wall beta limit according to ideal MHD calculations. The mismatch is minimised by applying a new way of determining the RFA threshold, based on evaluating the logarithmic derivative of the RFA amplitude as a function of the normalised plasma pressure. This improved method is shown, at least in theory, to be robust in predicting the no-wall beta limit for JET plasmas.

1. INTRODUCTION

The effects of error fields on the stability and confinement of tokamak plasmas have been known for a long time. Passive or active error field correction, using magnetic coils, has been proved an efficient way to improve the plasma performance in many present tokamaks. It is also foreseen as an important design aspect in ITER [1].

It was, however, only recently realised that the plasma response can play a crucial role in amplifying the external, static magnetic fields, due to the existence of meta-stable, low-n, low frequency MHD modes in the plasma [2]. One example is the resonant field amplification (RFA) caused by the Resistive Wall Mode (RWM), marginally stabilised by the plasma rotation or kinetic effects. For a linear plasma response, the RFA is defined as the field contribution from the plasma, measured at a certain radius and normalised by the corresponding resonant vacuum (error) field in the absence of the plasma. Theplasma RFA response generally involves an amplitude amplification and a toroidal phase shift with respect to the vacuum field. Normally a significant RFA due to the RWM occurs in high pressure plasmas. Taking into account the field amplification factor will effectively reduce the error field threshold predicted for ITER high performance scenarios.

Another, no less important consequence of RFA is the enhanced detrimental effect on the plasma momentum confinement. For instance, the plasma toroidal rotation in a tokamak can be reduced by a torque from the Neoclassical Toroidal Viscous (NTV) force [3], which depends quadratically on the amplitude of the non-axisymmetric field perturbations inside the plasma. The RFA can contribute a substantial portion to these field perturbations. Experimental evidence of strong NTV braking has been recently reported [4]. This is in contrast with the conventional understanding of rotational damping via resistive layer response [5]. Because of the substantial role of the plasma rotation played in both stability and confinement of tokamaks including ITER, a good understanding of RFA and RFA-induced momentum damping is essential.

Extensive RFA measurements have recently been performed in experiments. It is established in both DIII-D [6, 7, 8, 9, 10] and JET [11, 12, 13, 14] experiments that the field amplification due to the RWM is monotonically enhanced with increasing the plasma pressure beyond the no-wall beta limit. A significant effort of cross-machine comparison has also been carried out [15]. Further, the ac field induced RFA has been proposed as a MHD spectroscopy tool, for measuring the damping

rate and real frequency of the RWM [9, 10]. We also mention that RFA has been accurately measured and modelled in reversed field pinch experiments [16].

Theory and modelling work for understanding the resonant field amplification phenomenon have been on-going during recent years [17, 18, 19, 20, 13, 21]. An important result is that the ideal MHD theory (with Alfvén or sound wave continuum damping) for the RWM [12, 19] cannot explain the qualitative behaviour of RFA versus the plasma pressure, observed in experiments. Additional damping beyond the ideal MHD description is required to explain the experiments. Quantitative agreement is achieved between theory and experiments by considering a strong parallel sound wave damping model, or a more physics based, semi-kinetic damping model [13].

In this work, the RFA is defined, in both modelling and experiments, in the following way. Applying a coil current in the form of a standing wave (with an excitation frequency ω_{ext})

$$I_{coil}(t) = I_0 \sin \omega_{ext} t,$$

a set of detection coils measures the radial magnetic flux with and without the plasma, respectively. The n = 1 toroidal Fourier component of the flux are identified at two toroidal locations, separated by 90^o toroidally. For the radial flux measured at the same toroidal location as the field-generating coils (antenna coils), we denote the wall response (i.e. in the absence of the plasma) by

$$\psi_{vac,a}(t) = \psi^0_{vac,a}(\omega_{ext}) \sin(\omega_{ext} t - \varphi_{vac,a})$$

where $\varphi_{vac,a}$ is the temporal phase delay caused by the image currents in the wall. The total flux with the plasma (and the wall) response is defined in a similar manner

$$\psi_{vac,a}(t) = \psi^0_{vac,a}(\omega_{ext}) \sin(\omega_{ext} t - \varphi_{vac,a})$$

When we measure the flux at a 90^o-shifted toroidal angle with respect to the antenna coils, an axi-symmetric wall alone gives a vanishing contribution. The plasma response, however, does yield a finite contribution, due to the toroidal plasma rotation and/or damping effects on the stable mode (the resistive wall mode in this study) that is present in the plasma. This response, causing a spatial phase shift with respect to the coil current, is denoted by

$$\psi_{tor,r}(t) = \psi^0_{tor,r}(\omega_{ext}) \sin(\omega_{ext} t - \varphi_{tor,r})$$

We note that all quantities are real numbers in the above equations. A general experimental definition of RFA is given in [9, 10]. A simpler definition is used in JET experiments with external coils, since in this case $\psi^0_{vac,a} \simeq \psi^0_{tor,r}$ due to two facts: (i) as will be shown in the next Section, the sensor coils are well aligned with the antenna coils along the poloidal angle, and radially very close to the JET

vacuum vessel, detecting dominantly the field contributions generated by the wall and the antenna coil currents; (ii) at low plasma pressures, the plasma response field is weak compared with the direct vacuum field from the coils. Therefore, a practical definition of the RFA amplitude, from the JET experimental point of view, is

$$|\mathrm{RFA}|\,(\omega_{ext}) \equiv \frac{\psi^0_{tot,r}\,(\omega_{ext})}{\psi^0_{tot,a}\,(\omega_{ext})}\,.$$

This is the definition followed both in the experiments and in the present modelling.

This work will not focus on studying the RFA beyond the no-wall beta limit. Instead, we investigate the plasma response, observed in JET discharges, that occur before the plasma pressure reaches the no-wall limit. The motivation is given by Fig.1. This figure shows the growth rates (solid lines) of the n = 1 ideal kink mode, computed for three different JET plasmas. The marginal stability corresponds to the no-wall beta limit, in terms of the normalised beta $\beta_N \equiv \beta(\%)a(m)B_0(T)/I_p(MA)$. The MARS-F code [22] is used for these calculations. Very similar limits are predicted [23] by the MHD code MISHKA-1 [24]. Three vertical (dash-dotted) lines indicate the measured n = 1 RFA threshold from experiments. The RFA threshold is defined as the β_N value giving the minimum of the curve $|\mathrm{RFA}|/\beta_N$ as a function of β_N. (Details are shown in Fig.3.) We observe a systematic, large downward shift of the RFA-measured thresholds compared to the beta limits according to the ideal MHD theory. This shift cannot be explained by the plasma toroidal rotation in JET, which is a few percent of the Alfv´en speed in these discharges. This rotation speed does not have a significant effect on the stability of the ideal kink mode. It does, however, affect strongly the stability of the RWM, which is completely stabilised by rotation in these experiments. Our purpose here is to establish the correlation between the stability limit of the kink mode, and the RFA threshold, which is expected to be due to the response of the stable RWM.

2. MODELLING RESULTS

Figure 2 shows the geometrical configuration of the RFA simulations with MARS-F. An axi-symmetric, complete, thin shell is used to approximate the conducting wall (vacuum vessel) in JET, with the realistic (non-conformal) wall shape. We point out that in the JET machine there are also conducting structures located between the plasma surface and the vacuum vessel, as well as between the vacuum vessel and the external antenna coils. These structures are not distributed axi-symmetrically along the toroidal angle, and can have a non-negligible influence on the measured RFA response under ac conditions [25].

The radial and poloidal location of the Error Field Correction Coils (EFCCs) and the sensor coils (close to the wall) are indicated by squares in Fig.2. These coils are modelled by saddle loops located at the same radial and poloidal position, but of a sufficiently large number along the toroidal angle ϕ, such that the $\exp(in\phi)$ field pattern is produced by these coils. This is normally not a strong assumption, since e.g. 6 saddle coils can generate very well a dominant n = 1 field. We note that

JET has only 4 error field correction coils along the toroidal angle, which makes our assumption marginally applicable. The most significant consequence, in comparing the experimental data with the simulation results, is the necessity of mapping out the equivalent n = 1 contribution from the experimental total coil current.

The sensor coils detect the radial flux. In the JET experiments, the integrated coil signals at a toroidal angle, 90 degrees shifted with respect to the EFCC currents, is used as the RFA response from the mode.

Normally in order to model a β_N scan, we scale the amplitude of the plasma pressure while keeping the pressure and current profiles fixed. The total plasma current is also fixed. Figure 3 shows the computed RFA for equilibria reconstructed from three JET pulses as in Fig.1. The three curves in the figure show the RFA amplitude, divided by β_N, versus β_N. The N values, corresponding to the minimum of these curves, are defined as the RFA thresholds as in the experiments [23]. The measured thresholds, indicated again by vertical dash-dotted lines in Fig.3, agree reasonably well with the simulation results. The important point is that these thresholds are systematically below the no-wall beta limits from ideal calculations, as indicated by the solid vertical lines in the figure. The difference in β_N is about 1 but varies with equilibria. This circumstancemakes it difficult to use the RFA measurement to predict the 'true' stability limit for the ideal kink. Hence we seek for a new definition of the RFA threshold, that can better match the no-wall beta limit.

One of the possibilities, that we have found numerically, is described by Fig.4. Using the same computed RFA data as shown in Fig.3, we compute the logarithmic derivative of the RFA magnitude versus β_N. It turns out that the logarithmic derivative reaches its peak at a β_N very close to the corresponding no-wall limit. We notice that there are also local extrema shown in Fig. 4. This is because the logarithmic derivative is sensitive to the accuracy of the computed or measured RFA amplitude. These smaller local extrema are essentially noise due to the fact that a cubic smoothing spline is used to interpolate the computed RFA amplitude, prior to evaluating the logarithmic derivative. One obvious drawback of this technique is the requirement of high accuracy in the experimental RFA measurements. Nevertheless, this new technique of determining the RFA threshold seems to be robust against the way the RFA is excited, either by dc or ac currents flowing in the EFCCs.

We point out that although the computed RFA thresholds agree well with the experimental values as shown in Fig.3 for these JET pulses, the computed no-wall beta limits seem to be too large to match the RFA behaviour observed in experiments, as shown in Fig.5 for two of the pulses. This is thought to be largely due to the inaccuracy of the equilibrium reconstruction for these JET plasmas, since it is well understood that the no-wall beta limit for an ideal kink mode is sensitive to the plasma pressure and q profiles. This does not affect the conclusion that the computed maximum point of the logarithmic derivative $d\ln|RFA|/d\beta_N$ coincides with the computed no-wall beta limit, since both computations are performed consistently for the same set of (artificial) equilibria.

A more carefully tuned reconstruction procedure does result in a more accurate equilibrium for the JET plasma, which brings reasonable agreements between the experimental data and the

modelling results not only for the RFA threshold, but also for the no-wall beta limit. One example is shown in Fig.6, where the equilibrium q profile (the radial location of rational surfaces) is carefully calibrated by matching the measured plasma toroidal rotation frequency with the measured MHD (islands) rotation frequency, for JET Pulse No: 68875 [25]. [This technique assumes that the propagation of the mode with respect to the fluid is a small effect, and also that the correction of the velocity from the C^{6+} impurity measured rotation to the bulk deuterium velocity is small.] Figure 6 compares the computed RFA amplitude (lines), based on a set of equilibria for Pulse No: 68875, with the measured values (dots) from three similar discharges including Pulse No: 68875. In the simulation, we have to vary the wall penetration time τ_w for the 2D thin shell as shown in Fig.6, in order to approximately take into account the effect of 3D conducting structures located between the plasma surface and the EFCCs. We make this approximation since the MARS-F code can represent only toroidally uniform (i.e. 2D) walls. At a finite EFCC frequency (10Hz in these JET pulses), the induced eddy currents in these 3D conducting structures effectively increase the wall penetration time.

Figure 6 shows that one can choose an 'equivalent' wall time constant (25ms in this case), for which the simulated RFA amplitude matches well the experimental value. More noticeably, even if we relax the requirement on matching the RFA amplitude (hence the wall time tuning), we still obtain a good agreement between the computed and the measured RFA threshold (about $\beta_N = 2.4$ in this case). According to the stability calculation for the n = 1 ideal kink mode, the no-wall beta limit is about 2.6 for the JET Pulse No: 68875. This limit is again well reproduced by the computed RFA response, by evaluating the logarithmic derivative of the RFA amplitude, as shown in Fig.7, which also shows that this definition is not sensitive to the choice of the wall time constant.

Further modelling results also show that the new logarithmic definition of the RFA threshold, for the purpose of predicting the no-wall beta limit, is robust not only against the wall time constant, but also against the wall geometry (even double wall structures used to model the JET conducting structures). Moreover, the robustness seems to persist with variation of several plasma related parameters, for instance, the plasma rotation, the equilibrium edge current pedestal, and the models for simulating the RWM damping. Figure 8 shows one example, where the plasma rotation speed is varied. Both dc and ac excitation conditions are considered. The MARS-F computed RFA threshold, according to the new definition, agrees reasonably well with the computed no-wall beta limit in all cases.

Another example of the robustness is shown in Fig.9. The plasma equilibria, that we used for obtaining the results in this figure, are different from those we used so far, in the sense that a finite equilibrium current density at the plasma edge is retained in the former, which leads to instability of an n = 1, ideal peeling mode at the plasma edge. For the specific series of equilibria studied in Fig.9, the peeling mode is unstable for $\beta_N < 0.45$, and stable for $\beta_N > 0.45$. A detailed study of the peeling mode stability and resonant response will be reported elsewhere [26]. Here we are interested in the plasma response near the no-wall limit $\beta_N = 2.51$, where the peeling mode contribution is small, and most of the RFA response comes from the stable n = 1 RWM. Figure 9 shows three

cases, with different degrees of damping assumed in the MARS-F computation. We adopt the sound wave damping model, that introduces a viscous force to effectively mimic the ion Landau damping of the parallel sound wave [27]. A numerically adjustable coefficient $k_{\|}$ is introduced in this model to prescribe the degree of damping. Our previous numerical experience shows that a $k_{\|}$ value above 1 but not very far from unity leads to the RWM damping that describes reasonably well the experimental situation. [We assumed $k_{\|} = 1.5$ for results reported in other figures.] By varying the $k_{\|}$ value from 1 to 2, we notice that the peaks of logarithmic derivatives of the computed RFA amplitude stay reasonably well near the computed no-wall beta limit.

As a final and important remark on the above modelling results for JET, we point out the difficulty of matching the MARS-F computed RFA amplitude with the experimental data.

First of all, we notice that with a single, complete wall model (with the same shape and position as the JET vacuum vessel), we have to assume a much larger wall time constant, of 25ms as shown in Fig. 6, in order to match the RFA amplitude. The field penetration time for the JET vacuum vessel is estimated to be a few milliseconds. Moreover, a single-wall model does not lead to a reasonable match of even the JET vacuum data (i.e. the measured frequency response of the conducting structures to EFCCs or internal saddle coil currents, in the absence of the plasma). Adding a second, complete wall between the plasma and the EFCCs, with a free choice of the wall time constant, does not result in a satisfactory agreement for the vacuum data. The only possible model, within the 2D complete wall approximation, is to have the second (thin or thick) wall located beyond the EFCCs, as shown both by extensive MARS-F simulations and by a simple cylindrical analysis [25].

This double-wall model allows a good match of all the vacuum data. The time constant of the inner wall (corresponding to the JET vacuum vessel) can be chosen to be the realistic value, while the time constant for the outer, fictitious wall has to be chosen an order of magnitude larger. Even with this double-wall model, a good match of the plasma response requires that the vertical separation between the outboard midplane sensor coils and the magnetic axis needs to be increased by about 15cm in the simulation. This is qualitatively understandable since the plasma response field, as a result of the kink-ballooning nature of the RWM eigenstructure, varies sharply near the outboard midplane. This makes the plasma response flux sensitive to either the plasma position with respect to the sensor or the exact details of the eigenstructure at the edge. In addition local 3-D conducting structures will contribute. This small discrepancy is not expected to undermine the method.

A wall structure outside the EFCCs does not correspond to the physical arrangement of conducting structures in JET. There are mechanical support structures inside the EFCC radius, and some of our previous modelling [12] indicated that it is possible to match the EFCC vacuum and RFA data by choosing such a second wall between the JET vacuum vessel and the EFCCs, but with a toroidal gap located at the outboard mid-plane.

These investigations lead to a conclusion that, for a realistic modelling of the RWM response in JET, without tuning parameters for the conducting structures, we need to consider a full 3D model

for JET walls. Accurate modelling of the RFA response with JET 3D conductors will be carried out in the near future, using a recently developed code CarMa [28, 29] that allows a detailed full 3D description of these structures.

3. AN ANALYTIC MODEL

To understand the simulation results from Section 2, we consider a simple analytic model proposed by Fitzpatrick and Aydemir [30, 31]. According to this model, the growth rate of the RWM, subject to boundary layer viscous damping in a rotating plasma, satisfies the following cubic dispersion relation

$$\left[(\hat{\gamma} - i\hat{\Omega}_\phi)^2 v_*(\hat{\gamma} - i\hat{\Omega}_\phi) + (1 - \kappa)(\gamma - md)\right](\hat{\gamma}S_* + 1 + md) = 1 - (md)^2, \quad (1)$$

where $\hat{\gamma}$ is the normalised growth rate of the mode, $\hat{\Omega}_\phi$ the normalised toroidal rotation frequency of the plasma, v_* normalised viscosity coefficient. The intrinsic stability of the plasma in the absence of rotation is measured by the parameter κ, such that $\kappa = 0$ corresponds to the no-wall limit of ideal kink, and $\kappa = 1$ corresponds to the ideal-wall limit. For the pressure driven RWM, a parameter $C_\beta \equiv (\beta_N - \beta_N^{\text{no-wall}})/(\beta_N^{\text{ideal-wall}} - \beta_N^{\text{no-wall}})$, similar to , is normally introduced, where $\beta_N^{\text{no-wall}}$ is the no-wall limit, and $\beta_N^{\text{ideal-wall}}$ is the ideal-wall limit for the external kink mode.

In Eq. (1), m is the poloidal mode number, d a constant dependent of the wall minor radius. S_* measures the conductivity of the wall. We refer to [31] for the precise definitions of the parameters in the model.

For a given viscous damping coefficient v_*, the RWM is stabilised by the plasma rotation exceeding a critical value. For these stable RWM, we compute the RFA factor using an empirically verified formula [10]

$$\text{RFA} = C_g \frac{8 + \gamma\tau_w}{i\omega_{ext}\tau_w - \gamma\tau_w}, \quad (2)$$

where C_g is a geometrical factor, ω_{ext} is the frequency of the external field. The real part of γ, computed as one root (the RWM branch) of the dispersion relation (1), measures the mode damping rate, and the imaginary part of γ measures the mode real frequencyin the laboratory frame.

Figures 10(a-d) show one example of determining the RFA threshold using the Fitzpatrick-Aydemir model. Note that we assume a strong damping regime for the RWM, with $v_* = 2$, though Eq. (1) was derived in [31] under the assumption of a weak dissipation $v << 1$. The experimental evidence [32, 13, 15] of the measured critical rotation versus C_β (or κ) seems to confirm that the model with a strong damping is more relevant in describing the RWM dynamics in most present tokamaks. Figure 10(a) shows the damping rate and frequency of the mode versus the stability index κ. At a sufficient plasma rotation, the RWM is stable for all κ values. We should point out that, for κ very close to 1 (the ideal-wall limit), the model gives an unstable branch that cannot be

stabilised by any rotation. This unphysical branch is neglected here.

Another argument for the choice of large v_* in the model is the RFA behaviour versus C_β. The RFA amplitude measured in both DIII-D [7, 15] and JET [13] increases monotonically with increasing C_β, whilst the Fitzpatrick-Aydemir model with $v_* << 1$ (as well as other RWM models assuming only MHD type of damping) results in the peaking of the RFA amplitude around $C_\beta = 0$. However, at sufficiently strong dissipation and fast plasma rotation, the model does predict a RFA behaviour resembling experimental measurements, as shown by Fig.10(b). We define and investigate the RFA threshold only for these parameter regimes.

Figure 10(c) shows the RFA magnitude, normalised by β_N, versus κ. We assume a simple linear relation between β_N and κ: $\beta_N = 2 + \kappa$. (The RWM in the Fitzpatrick- Aydemir model is current driven, hence no "true" β_N can be defined.) The qualitative behaviour shown in Fig. 10(c) does not depend on the exact choice of the relation between β_N and κ. We observe a minimum value at below 0, or converted in the pressure limit, at β_N below the no-wall limit. This is exactly the behaviour found in the JET experiments and in the MARS-F simulations (Fig.3). Using the new definition for the RFA threshold, as that from Fig. 4, we find that the peak, shown in 10(d), also occurs at the no-wall limit $\kappa = 0$ according to this analytic model.

The exact match between the RFA threshold and the no-wall limit, as shown in 10(d), does not always happen in the Fitzpatrick-Aydemir model. It happens only when the plasma dissipation and rotation are tuned in such a way, that the RFA dependence on κ, as shown by 10(b), matches the experimental (monotonic) behaviour across the no-wall limit $\kappa = 0$. Figure 11 shows a domain (shaded region) in the $\Omega - v_*$ plane, where the RFA threshold, determined by the peak of the logarithmic derivative curve, matches the no-wall limit within $\kappa = \pm 0.1$, or within 5% error in $\beta_N = 2 + \kappa$. This is a reasonably large domain in both the damping coefficient v_* and the plasma rotation frequency , showing the robustness of the new definition of the RFA threshold against variation of rotation and damping. This also confirms the findings from the toroidal modelling results.

CONCLUSION AND DISCUSSION

The effect of resonant field amplification, due to the response of the low-n RWM to the externally applied magnetic fields, is modelled for JET plasmas using the MARS-F code.

The modelling focuses on the RFA threshold measured in JET discharges. The simulation results confirm a systematic shift of the RFA onset pressure, defined by the minimum of $|RFA|/\beta_N$, from the predicted no-wall beta limit by ideal MHD theory. A new technique of using the RFA data to recover the no-wall beta limit is proposed, based on the MARS-F results. This technique computes the logarithmic derivative of the RFA amplitude as a function of β_N. The maximal point offers a better way to predict the no-wall beta limit. The prediction seems to be robust against the plasma equilibrium profiles, the toroidal rotation and damping models, as well as the wall characteristics. We point out that this procedure, although it works well in theory, may be difficult to apply in practice, since it requires accurate RFA measurements from experiments. Work is in progress to

experimentally verify this method.

A quantitative match of the modelled RFA amplitude with the JET data will require an accurate description of the JET walls. This can be achieved by considering the realistic 3D description of the JET conducting structures, without introducing any adjustable parameters for the wall model. Such studies are in progress using the CarMa code.

ACKNOWLEDGMENTS

Y.Q. Liu acknowledges many fruitful discussions with Dr. C.G. Gimblett from UKAEA Culham and Dr. V.D. Pustovitov from Kurchatov Institute during this work. We also thank the JET TF-M Leader Dr. H.R. Koslowski, and Dr. A.W. Morris from UKAEA Culham for valuable suggestions in improving the manuscript. This work was funded jointly by the United Kingdom Engineering and Physical Sciences Research Council and by the European Communities under the contract of Association between EURATOM and UKAEA. The views and opinions expressed herein do not necessarily reflect those of the European Commission. Work conducted within the framework of the European Fusion Development Agreement.

REFERENCES

[1]. Hender T.C. et al 2007 Nucl. Fusion **47** S128
[2]. Boozer A.H. 2001 Phys. Rev. Lett. **86** 5059
[3]. Shaing K.C. 2003 Phys. Plasmas 10 1443
[4]. Zhu W. 2006 Phys. Rev. Lett. **96** 225002
[5]. Fitzpatrick R. 1993 NF Nucl. Fusion **33** 1050
[6]. Okabayashi M. et al 2002 Plasma Phys. Controlled Fusion **44** B339
[7]. Garofalo A.M. et al 2003 Phys. Plasmas **10** 4776
[8]. Strait E.J. et al 2003 Nucl. Fusion **43** 430
[9]. Reimerdes H. et al 2004 Phys. Rev. Lett. **93** 135002
[10]. Reimerdes H. et al 2005 Nucl. Fusion **45** 368
[11]. Gryaznevich M.P. et al 2003 Bull. Am. Phys. Soc. **48** RP1.036
[12]. Hender T.C. et al 2004 Resistive wall mode studies in JET Proc. 20th IAEA Fusion Energy Conf. 2004 (Vilamoura, Portugal, 2004) (Vienna: IAEA) IAEA-CN-116/ EX/P2-22 CD-ROM file EX/P2-22
[13]. Hender T.C. et al 2006 Prediction of Rotational Stabilisation of ResistiveWall Modes in ITER Proc. 21st IAEA Fusion Energy Conf. 2006 (Chengdu, China, 2006) (Vienna: IAEA) IAEA-CN-149/ EX/P8-18 CD-ROM file EX/P8-18
[14]. Gryaznevich M.P. et al 2007 Experimental identification of the beta limit in JET Proc. 34th EPS Conference on Controlled Fusion and Plasma Physics 2007 (Warsaw, 2007) ECA 31A P1-070
[15]. Reimerdes H. et al 2006 Phys. Plasmas **13** 056107

[16]. Gregoratto D. et al 2005 Phys. Plasmas **12** 092510
[17]. Gimblett C.G. and Hastie R.J. 2004 Phys. Plasmas **11** 1019
[18]. Pustovitov V.D 2004 Plasma Phys. Rep. **30** 187
[19]. Zheng L. et al 2005 Phys. Rev. Lett. **95** 255003
[20]. Liu Y.Q. 2006 Plasma Phys. Controlled Fusion **48** 969
[21]. Pustovitov V D 2007 Nucl. Fusion **47** 563
[22]. Liu Y.Q. et al 2000 Phys. Plasmas **7** 3681
[23]. Gryaznevich M.P. et al 2008 Plasma Phys. Control. Fusion **50** 124030
[24]. Mikhailovskii A.B. et al 1997 Plasma Phys. Rep. **23** 844
[25]. Chapman I.T. et al 2009 Plasma Phys. Control. Fusion **51** 055015
[26]. Liu Y.Q. et al "Modelling resonant field amplification due to low-n peeling modes in JET" 2009 Plasma Phys. Control. Fusion to be submitted
[27]. Chu M.S. et al 1995 Phys. Plasmas **2** 2236
[28]. Albanese A. et al 2008 IEEE Trans. Mag. **44** 1654
[29]. Portone A. et al 2008 Plasma Phys. Control. Fusion **50** 085004
[30]. Fitzpatrick R. and Aydemir A.Y. 1996 Nucl. Fusion **36** 11
[31]. Fitzpatrick R. 2002 Phys. Plasmas **9** 3459
[32]. La Haye R.J. et al 2004 Nucl. Fusion **44** 1197

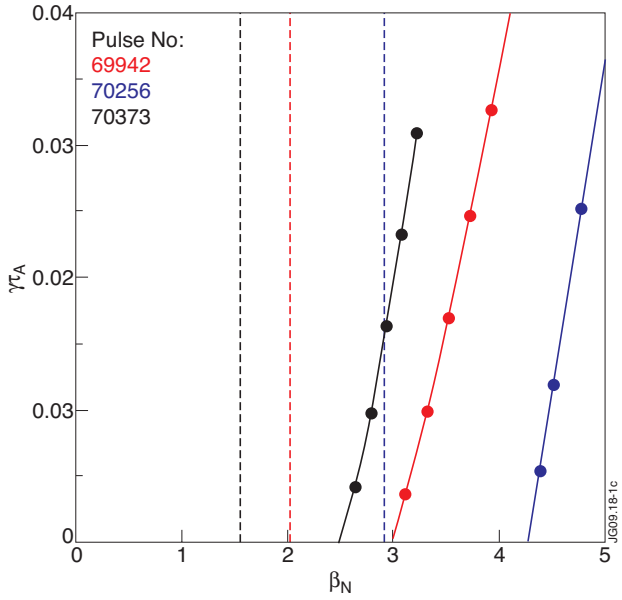

Figure 1: Growth rates (solid) of the n = 1 ideal kink mode versus β_N for three JET plasmas. The corresponding dash-dotted vertical lines indicate the measured n = 1 RFA threshold in experiments.

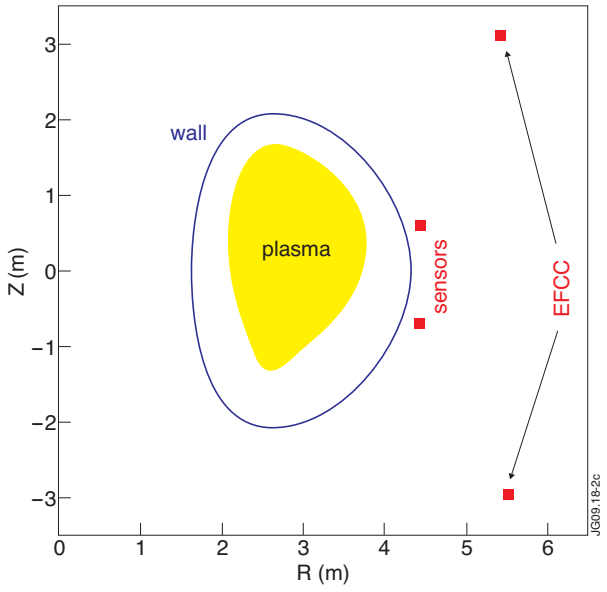

Figure 2: Geometry of the JET EFCCs and the magnetic pick-up coils modelled in MARS-F.

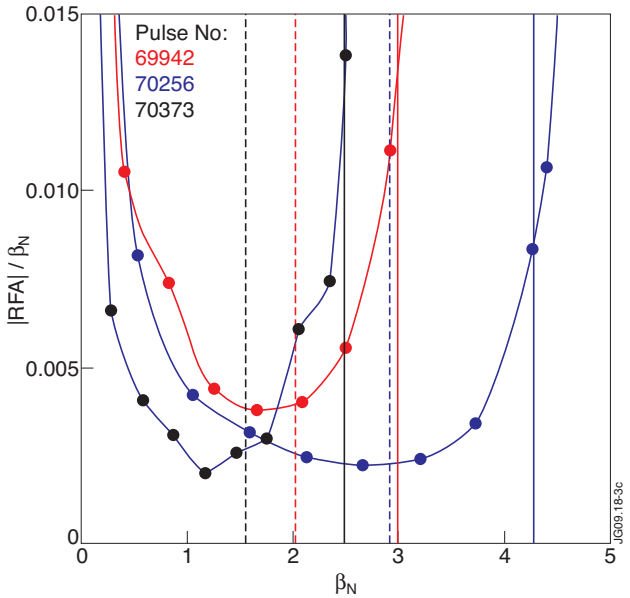

Figure 3: The normalised RFA amplitude versus β_N, computed by MARS-F for the plasmas from three JET pulses. The solid vertical lines indicate the computed no-wall beta limit for the ideal kink mode, whilst the dash-dotted vertical lines indicate the measured RFA threshold according to the experimental definition. A strong sound wave damping model is used in the simulations.

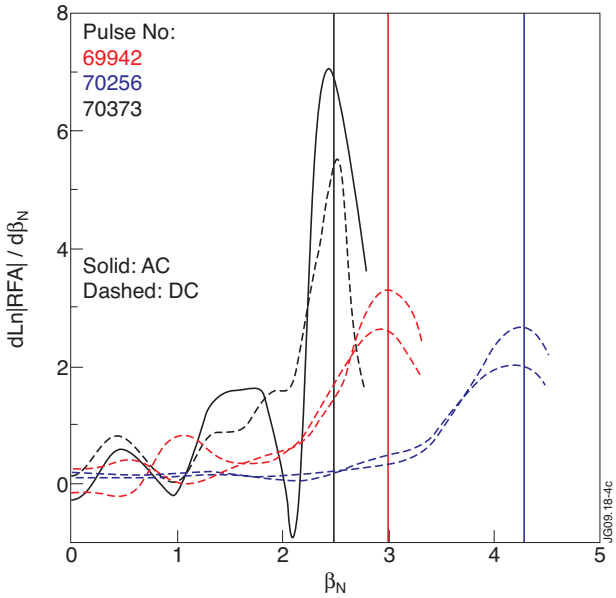

Figure 4: The new definition of the RFA thresholds matches well the no-wall beta limit, according to the MARS-F calculations. The curves are from the MARS-F simulation.

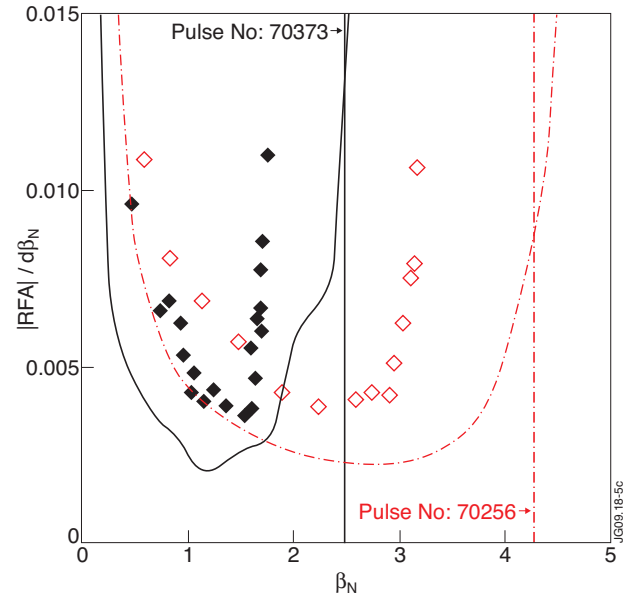

Figure 5: Comparison of the normalised RFA amplitude versus β_N between the MARS-F simulation (curves) and the experiments (dots), for two JET Pulse No's: 70256 and 70373. The solid vertical lines indicate the computed no-wall beta limits for the ideal kink mode. The difference between the simulation results and the experimental data, at higher β_N, is thought to be largely caused by the inaccuracy of the equilibrium reconstruction.

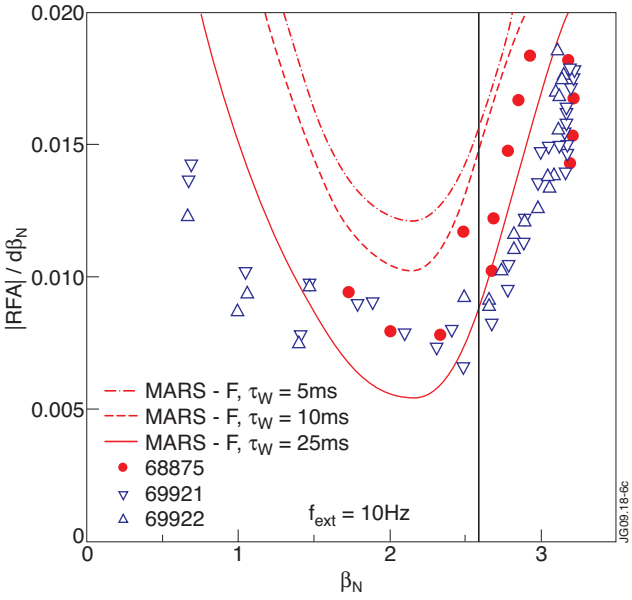

Figure 6: Comparison of the modelled RFA amplitude (curves) with the experimental data (dots) from three similar pulses. Simulation results obtained for an equilibrium reconstructed from Pulse No: 68875. Various values of the wall penetration time are assumed in the modelling, in order to take into account the eddy current effect of 3D metal supporting structures in JET. The solid vertical line indicates the computed no-wall beta limit for this equilibrium.

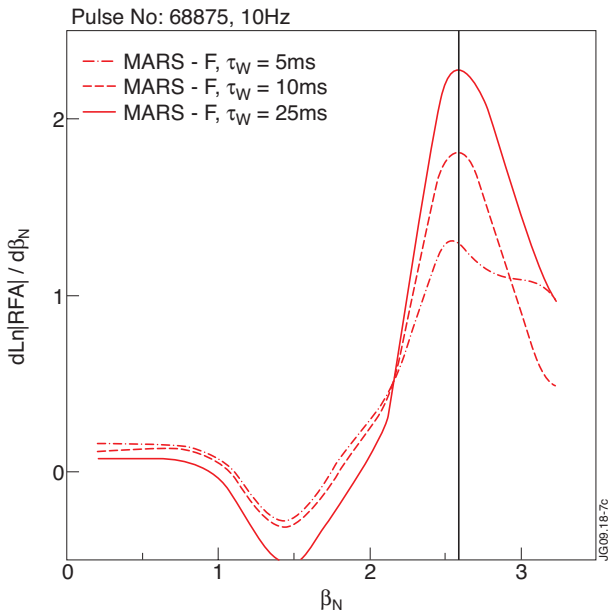

Figure 7: The new definition of the RFA threshold match well the no-wall beta limit for JET Pulse No: 68875, according to the MARS-F calculations.

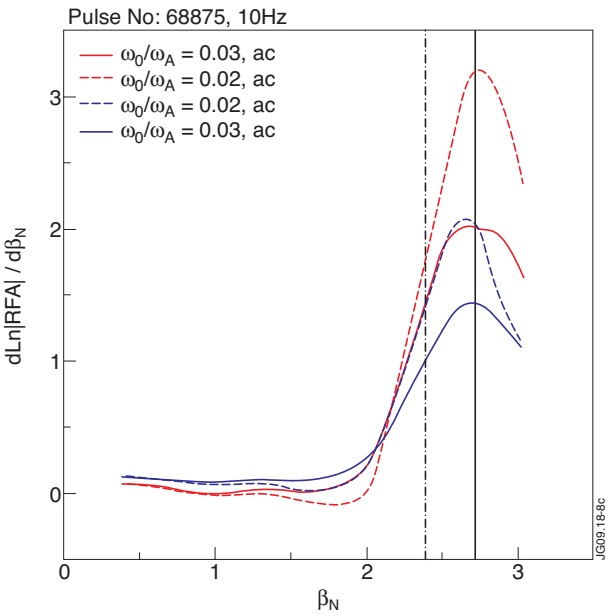

Figure 8: The new definition of the RFA threshold predicts well the no-wall beta limit against variation of the plasma rotation and the external field excitation frequency. The solid vertical line indicates the computed no-wall limit. The dash-dotted line indicates the RFA threshold according to the experimental definition. Results are computed by MARS-F for JET Pulse No: 68875.

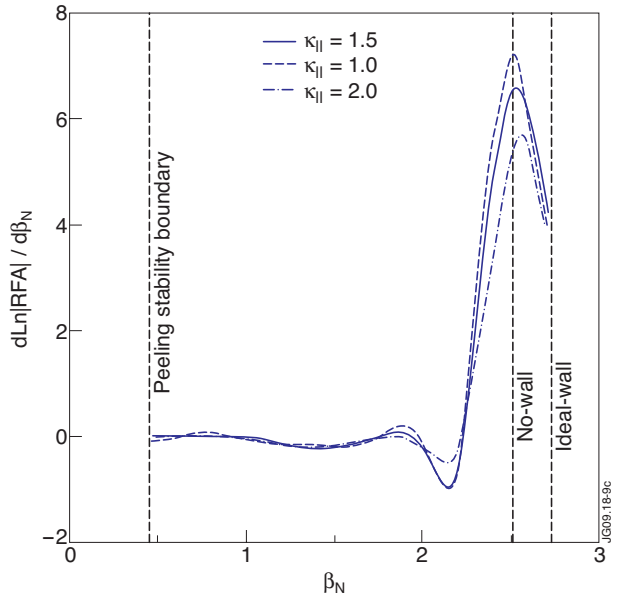

Figure 9: The new definition of the RFA threshold applied to equilibria from JET Pulse No: 70200, where a non-vanishing equilibrium current density at the plasma edge causes instability of the n = 1, ideal peeling mode at low plasma pressures. Three vertical dash-dotted lines indicate the peeling mode stability boundary $\beta_N = 0.45$, the no-wall limit $\beta_N = 2.51$ and the ideal-wall limit $\beta_N = 2.73$, respectively.

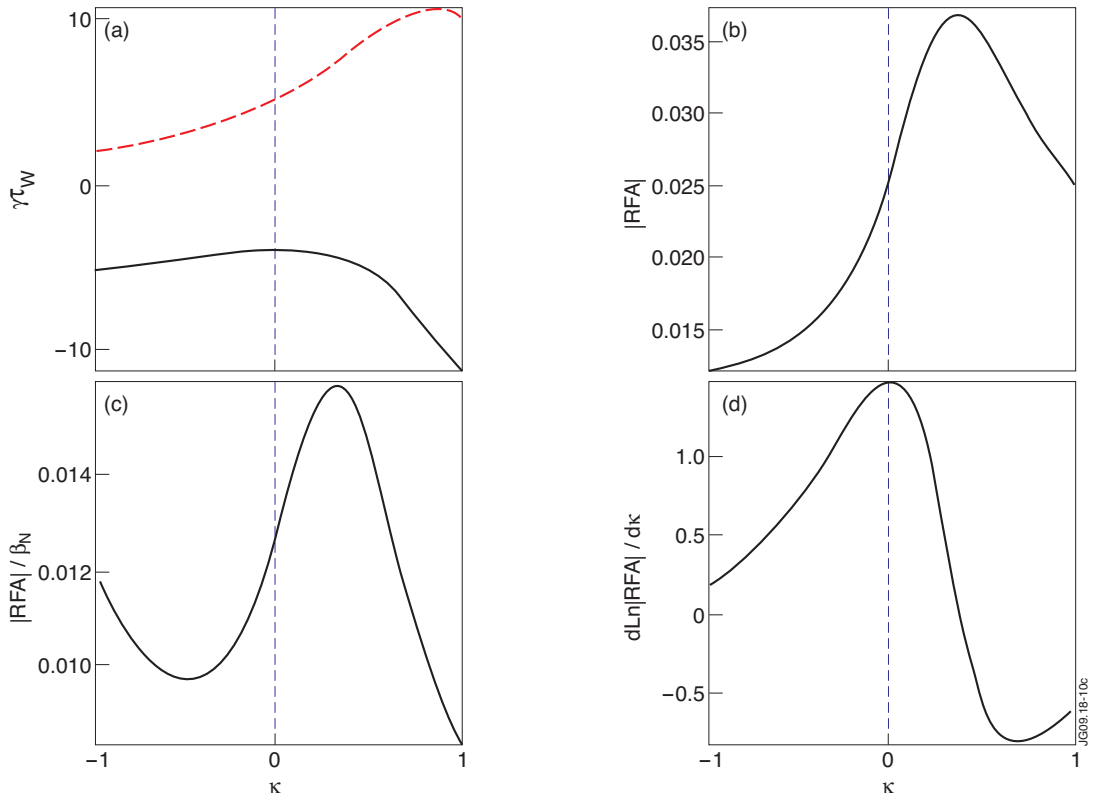

Figure 10: Different ways of defining the RFA threshold, for a plasma from the Fitzpatrick-Aydemir model with n = 1, m = 3, $v_* = 2$, $\Omega = 4.73 \times 10^{-3}\omega_A$, $r_w = 1.2a$, $\tau_w = 2.5 \times 10^4\ \tau_A$, $\omega_{ext} = 3\times 10^{-3}\omega_A$. (a) The real (solid) and imaginary (dashed) parts of the RWM damping rate; (b) the RFA amplitude versus the stability index κ; (c) the RFA amplitude normalised by β_N, where a simple relation $\beta_N = 2+\kappa$ has been assumed; (d) the new logarithmic derivative definition for the RFA threshold giving the same stability limit (the peak) at $\kappa = 0$, indicated by the vertical dash-dotted line.

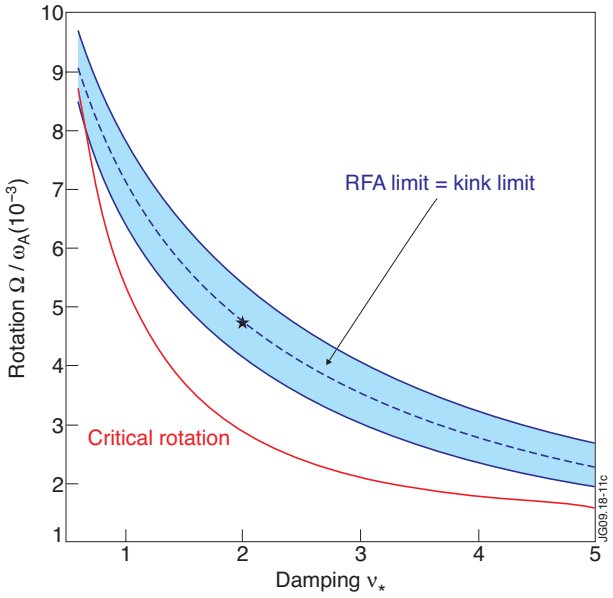

Figure 11: The region (shaded) in the rotation-damping domain, where the new definition of the RFA threshold matches the stability limit within $\kappa = \pm 0.1$, according to the Fitzpatrick-Aydemir model, for n = 1, m = 3, $r_w = 1.2a$, $\tau_w = 2.5\times 10^4\ \tau_A$, $\omega_{ext} = 3\times 10^4\ \tau_A$. The dashed curve corresponds to the exact match $\kappa = 0$. The RFA is defined and calculated in the stable region above the critical rotation curve, along which the RWM is marginally stable.